ELSEVIER

Journal of Fluids and Structures 21 (2005) 597–608

JOURNAL OF FLUIDS AND STRUCTURES

www.elsevier.com/locate/jfs

Torsional flutter and branch characteristics for 2-D rectangular cylinders

M. Matsumoto[a,b,*], K. Mizuno[c], K. Okubo[a], Y. Ito[a]

[a]*Department of Civil and Earth Resources Engineering, Kyoto University, Yoshida Honmachi, Sakyo-ku, Kyoto 606-8501, Japan*
[b]*Advanced Research Institute of Fluid Science and Engineering, Kyoto University, Kyoto, Japan*
[c]*West Japan Railway Company, Japan*

Received 25 May 2005; accepted 27 July 2005
Available online 20 October 2005

Abstract

Branch switching characteristics for coupled flutter and torsional flutter of structural sections are analyzed using step-by-step (SBS) flutter analysis. In the case of typical coupled flutter instability, prior to the appearance of flutter instability, the torsional branch (TB) controls the instability; although at certain lower velocity ranges after flutter onset, the TB and heaving branch (HB) coexist, with sudden switching in particular velocity ranges. In the vicinity of this velocity range, significant differences in the flutter characteristics are obtained by the conventional complex eigenvalue analysis (CEV) and the SBS methods, but in some velocity ranges, the two methods show good agreement. However, for flutter which is dominated by the TB, such as typical torsional flutter instability as for a 2-D rectangular cylinder with side-ratio B/D of 5 and 1.1 frequency ratio, $f_{\varphi 0}/f_{\eta 0}$, the flutter characteristics obtained by CEV and SBS analyses show fairly good agreement at all velocity ranges, where no branch switching is observed.

Keywords: Coupled flutter; Torsional flutter; Complex eigenvalue analysis; Step-by-step analysis; Branch switching

1. Introduction

With the development of aircraft since the Wright brothers' first flight in 1903, the flutter instability of wings had been a topic of research in the field of aeronautics. More recently, problems of flutter instability have been of interest in civil engineering, in particular the safe design of long span bridges. The problems of steady aerostatic force and unsteady aerodynamic force on thin plates, thin airfoils and structures have been studied by many scientists and researchers, including Theodorsen (1935), von Karman and Sears (1938) and Scanlan and Tomko (1971). An understanding of the mechanism for generation of flutter instability of bluff bodies is required in order to limit the flutter instability of flexible structures, such as long span bridges. Since the Tacoma Narrows Bridge failure in 1940, extensive research on flutter stabilization has been conducted, and at the present time the Akashi Kaikyo Bridge in Japan (main span length $l = 1991$ m, 1998) and the Great Belt East Bridge in Denmark ($l = 1624$ m, 1998) have been constructed, and even longer span bridges are being planned (e.g., Messina Strait Bridge, Italy, $l = 3300$ m). However,

*Corresponding author. Tel.: +81 75 753 5091; fax: +81 75 753 4911.
E-mail address: matsu@brdgeng.gee.kyoto-u.ac.jp (M. Matsumoto).

0889-9746/$ - see front matter
doi:10.1016/j.jfluidstructs.2005.07.021

some aspects of flutter instability of structures remain to be fully understood, and further research is needed in order for the next generation of long span bridges to be designed for more effective aerodynamic stabilization.

In this regard, for flutter instabilities of 2-D rectangular cylinders with various side ratios B/D, in the range of 5–20 (B: chord length, D: depth), the first author has previously shown that flutter characteristics change with the side ratio, B/D, due to the flow field around the cylinder during torsional or heaving vibration (Matsumoto et al., 1997a). In detail, B/D ratios of 5, 8, 10, 12.5, 15 and 20 change the flutter characteristics, such that the torsional flutter instability occurs for B/D equal to 5, 8 and 10, while coupled flutter occurs for $B/D = 12.5$, 15 and 20. The unsteady pressure characteristics of these cylinders, which are characterized by cylinder torsional/heaving motion, are fundamentally identical if they are measured in the nondimensional chord-wise coordinate with cylinder depth D, while the maximum unsteady pressure amplitude is proportional to the relative pitching angle induced by the torsional displacement, φ, and the heaving velocity, $\mathrm{d}\eta/\mathrm{d}t$. The unsteady pressure amplitude diagrams and the phase difference between body motion and unsteady pressure diagrams induced by the torsional motion of these cylinders are shown in Fig. 1 (Matsumoto, 1996).

The motion-induced lift and pitching moment can be characterized by integration of the unsteady pressure on the cylinder's upper and lower surfaces as the following equations:

For heaving motion:

$$L = \int_{-1}^{1} \tfrac{1}{2}\rho V^2 b\{-\tilde{C}_p \cos(\omega t - \Psi_H)\}\,\mathrm{d}x,$$
$$M = \int_{-1}^{1} \tfrac{1}{2}\rho V^2 b^2\{-\tilde{C}_p \cos(\omega t - \Psi_H)\}x\,\mathrm{d}x, \tag{1}$$

For torsional motion:

$$L = \int_{-1}^{1} \tfrac{1}{2}\rho V^2 b\{-\tilde{C}_p \sin(\omega t - \Psi_T)\}\,\mathrm{d}x,$$
$$M = \int_{-1}^{1} \tfrac{1}{2}\rho V^2 b^2\{-\tilde{C}_p \sin(\omega t - \Psi_T)\}x\,\mathrm{d}x, \tag{2}$$

where $\tilde{C}_p$is unsteady pressure amplitude, Ψ_H and Ψ_T are phase lag between heaving/torsional motion and pressure, x is pressure hole position, ρ is the air density, b is the half-chord length, and ω is the circular frequency.

Therefore, the flutter derivatives proposed by Scanlan and Tomko (1971) can be identified from these unsteady pressure characteristics. The heaving and torsional two-degree-of-freedom (2-dof) differential equations

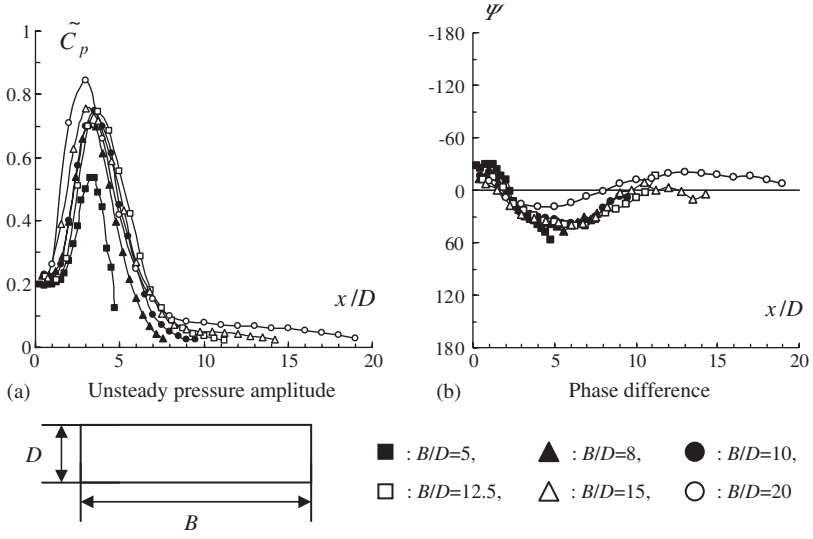

Fig. 1. Unsteady pressure characteristics of 2-D rectangular cylinders (torsional motion).

are expressed as follows:

$$m\ddot{\eta} + C_\eta\dot{\eta} + k_\eta\eta = \frac{1}{2}\rho(2b)V^2\left\{kH_1^*\frac{\dot{\eta}}{V} + kH_2^*\frac{b\dot{\phi}}{V} + k^2H_3^*\phi + k^2H_4^*\frac{\eta}{b}\right\}, \tag{3}$$

$$I\ddot{\phi} + C_\phi\dot{\phi} + k_\phi\phi = \frac{1}{2}\rho(2b^2)V^2\left\{kA_1^*\frac{\dot{\eta}}{V} + kA_2^*\frac{b\dot{\phi}}{V} + k^2A_3^*\phi + k^2A_4^*\frac{\eta}{b}\right\}, \tag{4}$$

where η and φ are the heaving and torsional displacements, m and I are the mass and mass inertia per unit span length, H_i^* and A_i^* ($i = 1-4$) are the flutter derivatives, and k is the reduced frequency ($k = b\omega/V$).

The eight flutter derivatives of these cylinders are shown in Fig. 2. By taking into account that the motion-induced unsteady pressure, or sequentially the motion-induced unsteady lift and pitching moment, is proportional to the relative pitching angle, the lift and pitching moment (which are proportional to torsional displacement, φ, and heaving velocity, $d\eta/dt$) can be classified as quasi-steady terms, while the torsional velocity, $d\varphi/dt$, and heaving displacement, η, can be thought of as unsteady terms. In particular, the torsional flutter instability can be generated by A_2^* having a positive value; therefore, the boundary between the torsional flutter and the coupled flutter must exist between $B/D = 10$ and 12.5, based on A_2^* characteristics. The torsional flutter, in consequence, can be classified as unsteady flutter. The positive or negative A_2^* is characterized by the center of gravity position of $C_pH_2^*$ relative to the mid-chord point of the cylinder. This means that if the center of gravity is located on the upstream side of the mid-chord point, then A_2^* is negative and coupled flutter occurs; while if the center of gravity is located on the downstream side from the mid-chord point, then A_2^* has a positive value and the torsional flutter instability occurs. Note that A_2^* changes smoothly and continuously from positive to negative with increasing B/D, and there is never a drastic change. However, it should be noted that the A_1^* and A_4^* characteristics for a B/D ratio of 5 differs from the characteristics for other B/D ratios. This is due to the different flow patterns around the oscillating cylinder—in detail, for $B/D = 5$, the cylinder does not have a stationary flow-reattachment type of the separated flow from the leading edge. For other B/D ratios, the cylinder has stationary flow-reattachment, which means that the separated flow from the leading edge always reattaches at any instant. In Fig. 3, the sensitivity of rectangular cylinders to torsional flutter and coupled flutter for B/D ratios of 5–20 is illustrated, while Fig. 4 shows the instability of coupled flutter, of cylinders which show coupled flutter instability, such as 2-D rectangular cylinders with B/D of 12.5–20, as a function of torsional and heaving frequency ratio, $f_{\varphi 0}/f_{\eta 0}$.

2. Flutter analysis

Currently, the complex eigenvalue analysis (CEV) method is widely used for flutter analysis, to solve for the four physical values of damping (δ), flutter frequency (f_F), heaving/torsional amplitude ratio (η_0/φ_0) and phase difference between heaving and torsional response (ψ). These four values are characteristic of the torsional branch (TB) and the heaving branch (HB), respectively, and are obtained from the eigenvalue analysis by the following equation:

$$[M]\{\ddot{z}\} + [C]\{\dot{z}\} + [K]\{z\} = [A]\{\dot{z}\} + [B]\{z\}, \tag{5}$$

where

$$[M] = \begin{bmatrix} m & 0 \\ 0 & I \end{bmatrix}, [C] = \begin{bmatrix} C_\eta & 0 \\ 0 & C_\phi \end{bmatrix}, \quad [K] = \begin{bmatrix} k_\eta & 0 \\ 0 & k_\phi \end{bmatrix}, \{Z\} = \begin{Bmatrix} \eta_0 \\ \phi_0 \end{Bmatrix} e^{\lambda t} = \{Z_0\}e^{\lambda t},$$

$$[A] = \begin{bmatrix} \rho b^2\omega H_1^* & \rho b^3\omega H_2^* \\ \rho b^3\omega A_1^* & \rho b^4\omega A_2^* \end{bmatrix}, \quad [B] = \begin{bmatrix} \rho b^2\omega^2 H_4^* & \rho b^3\omega^2 H_3^* \\ \rho b^3\omega^2 A_4^* & \rho b^4\omega^2 A_3^* \end{bmatrix}.$$

However, it is rather difficult to identify in which branch the coupled flutter instability occurs, if the CEV analysis is employed. This is because the formula to determine the complex frequencies, λ, for TB and HB is symmetric in terms of torsional and heaving motion, as follows:

$$\begin{aligned} &\lambda^4 + (2\zeta_\phi\omega_\phi + 2\zeta_\eta\omega_\eta)\lambda^3 + \left(4\zeta_\phi\zeta_\eta\omega_\phi\omega_\eta + \omega_\phi^2 + \omega_\eta^2\right)\lambda^2 \\ &\quad + \left(\omega_\phi^2 + \omega_\eta^2\right)\lambda + \left(\omega_\phi^2\omega_\eta^2\right) - (\rho b^2/m)(\rho b^3/I)\omega_F^2H_2^*A_1^*\lambda^2 \\ &\quad - \left[(\rho b^3/m)\omega_F^2H_3^* + (\rho b^2/I)\omega_F^2A_4^*\right]\lambda - \left[(\rho b^3/m)\omega_F^2H_3^* + (\rho b^2/I)\omega_F^2A_4^*\right] = 0, \end{aligned} \tag{6}$$

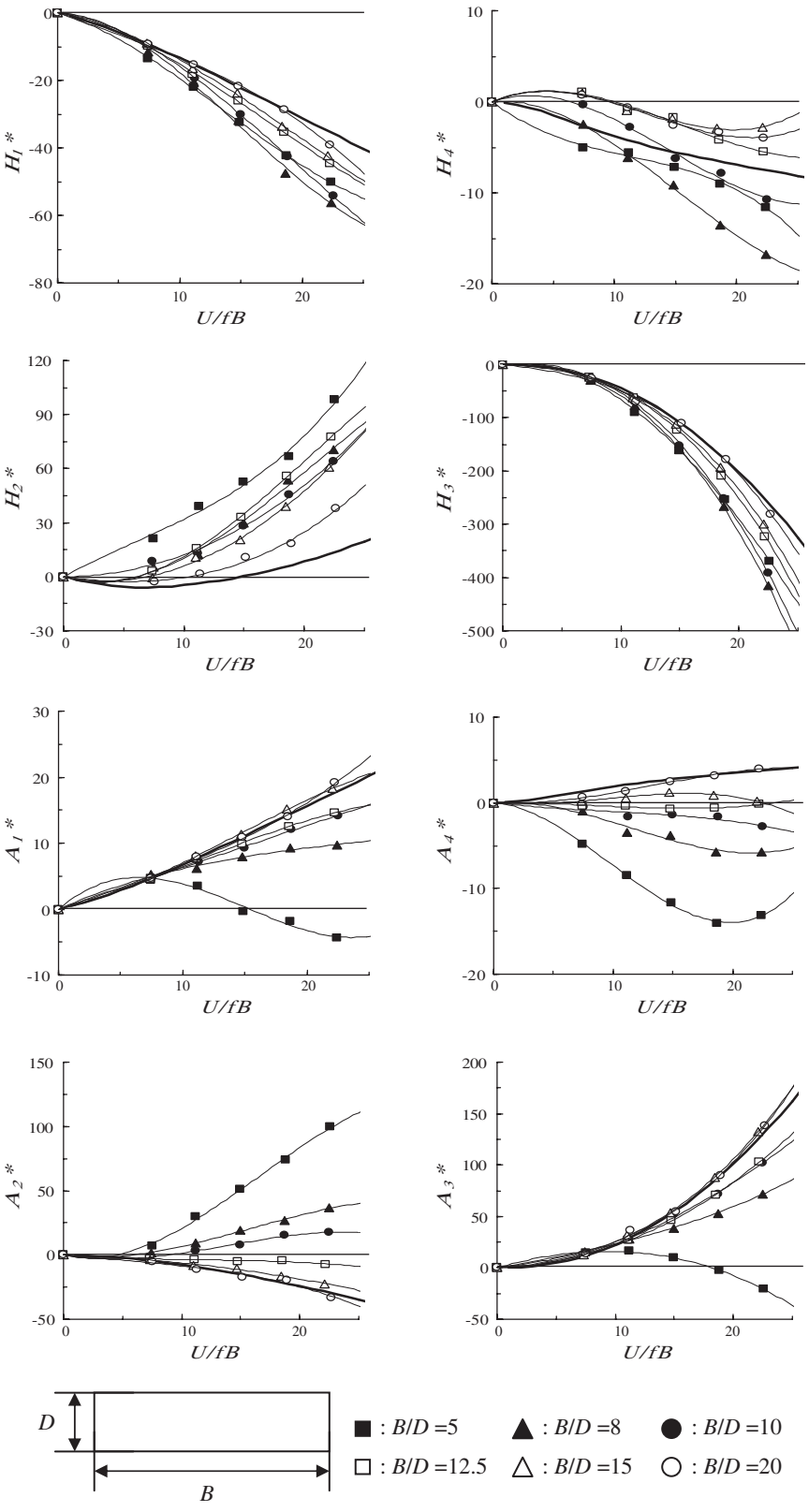

Fig. 2. Flutter derivatives of 2-D rectangular cylinders.

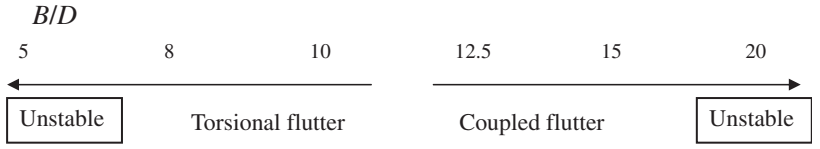

Fig. 3. Flutter sensitivity of 2-D rectangular cylinders with various side ratios, B/D.

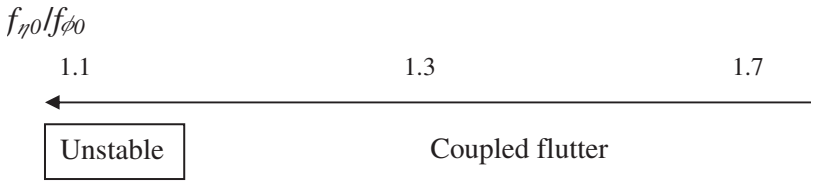

Fig. 4. Coupled flutter sensitivity of 2-D rectangular cylinders with various frequency ratios, $f_{\eta 0}/f_{\phi 0}$.

where $\omega_\varphi/\omega_\eta$ and ζ_φ/ζ_η are the torsional/heaving (circular) frequencies and damping (ratio) at V, respectively, which are affected by the noncoupled unsteady forces, and ω_F is flutter frequency.

The step-by-step analysis (SBS) method (Matsumoto et al., 1995, 1997a, b) can be used to clearly differentiate TB and HB flutter. The TB and HB flutter are determined if the final equation is controlled by the torsional differential equation of motion or the heaving differential equation of motion during the aerodynamic coupling between torsional and heaving motion, respectively. It is simply defined by the major controlling forces—that is, if unsteady pitching moment or unsteady lift is the major controlling force for flutter instability, then the flutter instability is classified as TB or HB, respectively. Furthermore, by taking into account the relative pitching angle, heaving motion in TB and torsional motion in HB determine the relative pitching angle, respectively. TB and HB flutter analysis in SBS analysis can be understood as follows.

2.1. TB flutter analysis

Step1. Torsional system (as initial motion)

Harmonic φ motion is assumed with φ_{0i} and $\omega_{\varphi i}$,

$$\phi = \phi_{0i} \sin(\omega_{\phi i} t);$$

coupled terms.

Step2. Heaving system (as forced vibration)

η response is generated with $\omega_{\varphi i}$, $(\eta_0/\varphi_0)_i$ and ψ_i,

$$\ddot{\eta} + \left(-\frac{\rho b^2}{m}\omega_F H_1^*\right)\dot{\eta} + \left(\omega_{\eta 0}^2 - \frac{\rho b^2}{m}\omega_F^2 H_4^*\right)\eta = \left(\frac{\rho b^3}{m}\right)\omega_F H_2^*\dot{\phi} + \left(\frac{\rho b^3}{m}\right)\omega_F^2 H_3^*\phi;$$

relative angle caused by η motion;

self-controlled uncoupled terms.

Step3. Torsional system (as free vibration)

$$\ddot{\phi} + \omega_{\phi i}^2\phi = \left(\frac{\rho b^4}{I}\right)\omega_F A_2^*\dot{\phi} + \left(\frac{\rho b^4}{I}\right)\omega_F^2 A_3^*\phi + \left(\frac{\rho b^3}{I}\right)\omega_F A_1^*\dot{\eta} + \left(\frac{\rho b^3}{I}\right)\omega_F^2 A_4^*\eta;$$

η and $\mathrm{d}\eta/\mathrm{d}t$ are replaced by φ and $\mathrm{d}\varphi/\mathrm{d}t$;

φ response is self-controlled with $\delta_{\varphi i+1}$, $\omega_{\varphi i+1}$,

$$\delta_{\phi i+1} = -XA_2^* - XY\{A_1^*|H_2^*|\cos\theta_1 + A_1^*|H_3^*|\cos\theta_2 - A_4^*|H_2^*|\sin\theta_1 - A_4^*|H_3^*|\sin\theta_2\},$$

$$\omega_{\phi i+1} = \sqrt{\omega_{\phi 0}^2 - (X/\pi)\omega_F^2 A_3^* - (XY/\pi)\omega_F^2\{A_1^*|H_2^*|\sin\theta_1 + A_1^*|H_3^*|\sin\theta_2 + A_4^*|H_2^*|\cos\theta_1 + A_4^*|H_3^*|\cos\theta_2\}},$$

where

$$X=\pi\left(\frac{\rho b^4}{I}\right),\ Y=\frac{(\rho b^2/m)\left(\omega_F/\omega_\eta^*\right)^2}{\sqrt{\left\{1-\left(\omega_F/\omega_\eta^*\right)^2\right\}^2+4\zeta_\eta^{*2}\left(\omega_F/\omega_\eta^*\right)^2}};$$

$\omega_{\varphi i}=\omega_{\varphi i+1}$?→if NO, then go to step1
if YES, then
Step4. Determination of flutter characteristic values (ω_F, δ_F, η_0/φ_0, ψ).

2.2. HB flutter analysis

Step1. Heaving system (as initial motion)
Harmonic η motion is assumed with η_{0i} and $\omega_{\eta i}$,
$\eta=\eta_{0i}\sin(\omega_{\eta i}t)$;
coupled terms.
Step2. Torsional system (as forced vibration)
φ response is generated with $\omega_{\eta i}$, $(\eta_0/\varphi_0)_i$ and ψ_I,

$$\ddot{\phi}+\left(-\frac{\rho b^4}{I}\omega_F A_2^*\right)\dot{\phi}+\left(\omega_{\phi 0}^2-\frac{\rho b^4}{I}\omega_F^2 A_3^*\right)\phi=\left(\frac{\rho b^3}{I}\right)\omega_F A_1^*\dot{\eta}+\left(\frac{\rho b^3}{I}\right)\omega_F^2 A_4^*\eta;$$

relative angle caused by φ motion;
self-controlled uncoupled terms.
Step3. Heaving system (as free vibration)

$$\ddot{\eta}+\omega_{\eta i}^2\eta=\left(\frac{\rho b^2}{m}\right)\omega_F H_1^*\dot{\eta}+\left(\frac{\rho b^2}{m}\right)\omega_F^2 H_4^*\eta+\left(\frac{\rho b^3}{m}\right)\omega_F H_2^*\dot{\phi}+\left(\frac{\rho b^3}{m}\right)\omega_F^2 H_3^*\phi;$$

φ and $\mathrm{d}\varphi/\mathrm{d}t$ are replaced by φ and $\mathrm{d}\varphi/\mathrm{d}t$;
η response is self-controlled with $\delta_{\eta i+1}$, $\omega_{\eta i+1}$,

$$\delta_{\eta i+1}=-XH_1^*-XY\left\{H_2^*|A_1^*|\cos\theta_1+H_2^*|A_4^*|\cos\theta_2-H_3^*|A_1^*|\sin\theta_1-H_3^*|A_4^*|\sin\theta_2\right\},$$

$$\omega_{\eta i+1}=\sqrt{\omega_{\eta 0}^2-(X/\pi)\omega_F^2 H_4^*-(XY/\pi)\omega_F^2\left\{H_2^*|A_1^*|\sin\theta_1+H_2^*|A_4^*|\sin\theta_2+H_3^*|A_1^*|\cos\theta_1+H_3^*|A_4^*|\cos\theta_2\right\}},$$

where

$$X=\pi\left(\frac{\rho b^2}{m}\right),\ Y=\frac{(\rho b^4/I)\left(\omega_F/\omega_\phi^*\right)^2}{\sqrt{\left\{1-\left(\omega_F/\omega_\phi^*\right)^2\right\}^2+4\zeta_\phi^{*2}\left(\omega_F/\omega_\phi^*\right)^2}};$$

$\omega_{\eta i}=\omega_{\eta i+1}$?→if NO, then go to step1
if YES, then
Step4. Determination of flutter characteristic values (ω_F, δ_F, η_0/φ_0, ψ).

In this study, a frequency convergence condition was employed with a 10^{-8} difference in frequency from the former step. The coupled flutter characteristics of a certain structural girder obtained by CEV analysis and SBS analysis are compared in Fig. 5. In this figure, the flutter characteristics obtained by two different analyses, CEV and SBS, show good agreement at all wind velocity ranges. On the other hand, the coupled flutter characteristics of a thin plate are shown in Fig. 6. In this figure, a drastic difference can be observed at higher velocities, for the point of branch switching. The SBS analysis shows the branch switching at a particular reduced velocity, at which flutter frequencies due to both TB and HB by the CEV analysis are shown. Furthermore, if the *V–f* diagrams for each 1-dof torsional/heaving system are compared with those of the 2-dof system, as shown in Fig. 6, the two frequency curves cross, similar to those

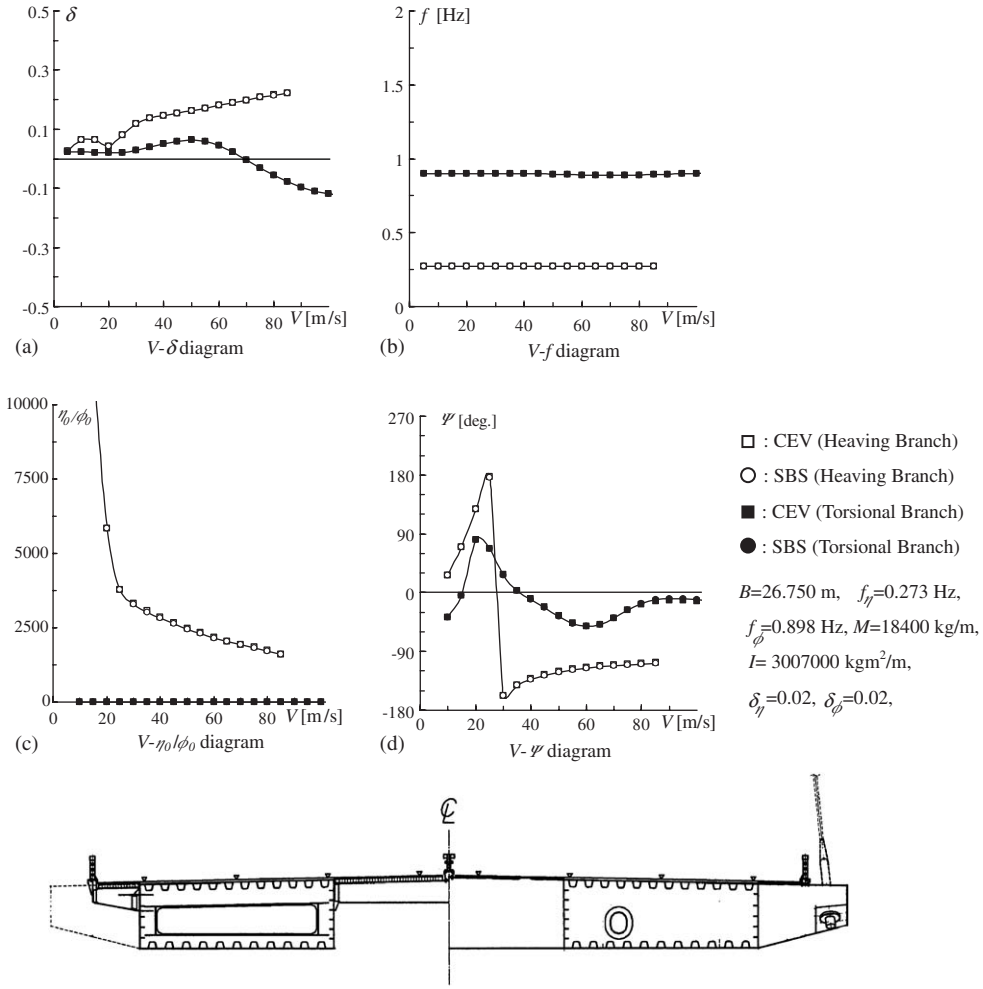

Fig. 5. Comparison of coupled flutter characteristics of a certain structural girder obtained by CEV and SBS analyses.

obtained by SBS analysis but not like those obtained by CEV analysis. The branch characteristics obtained by SBS analysis can be confirmed by direct measurement of the coupled flutter characteristics, measured by free vibration test in smooth flow for a rectangular cylinder with a side ratio of 20, as shown in Fig. 7. Then, by comparison with the characteristics of a 1-dof system, and with free vibration test for a rectangular cylinder with a side ratio of 20, it is seen that the branch switching, which can be predicted by SBS analysis, can actually occur. However, the solution by CEV analysis also indicates similar values as those of SBS analysis at lower velocities and at higher velocities, despite the branch difference. The physical meaning of the solution by CEV analysis at this particular reduced velocity range should be further investigated in the future.

Therefore, SBS analysis showed that the flutter branch switched from TB to HB for coupled flutter instability before/after the flutter instability appearance, and the flutter instability is controlled by HB. Based on SBS flutter analysis, the typical coupled flutter mechanism is illustrated in Fig. 8, by taking the branch switch into account. In particular, it should be noted that during the flutter branch switch process, coexisting velocity ranges for both TB and HB branches exist. For TB flutter stabilization, it is known that A_2^*, A_1^* and H_3^* control is rather effective (Matsumoto et al., 1997b); but using this branch switch another flutter stabilization can be proposed, which is by H_1^*, A_1^* and H_3^* control. These three derivatives are quasi-steady terms, which means that HB coupled flutter after flutter occurrence can be classified as a quasi-steady flutter. Therefore, coupled flutter appears as a branch switch from TB to HB. However, the problem of torsional flutter as a branch switch remains, because torsional flutter should be substantially controlled by the unsteady pitching moment. This flutter type is characterized by A_2^*, as described above, and the positive or negative of A_2^* is determined by the location of the center of gravity of $C_pH_2^*$ on the upstream or downstream side from the mid-

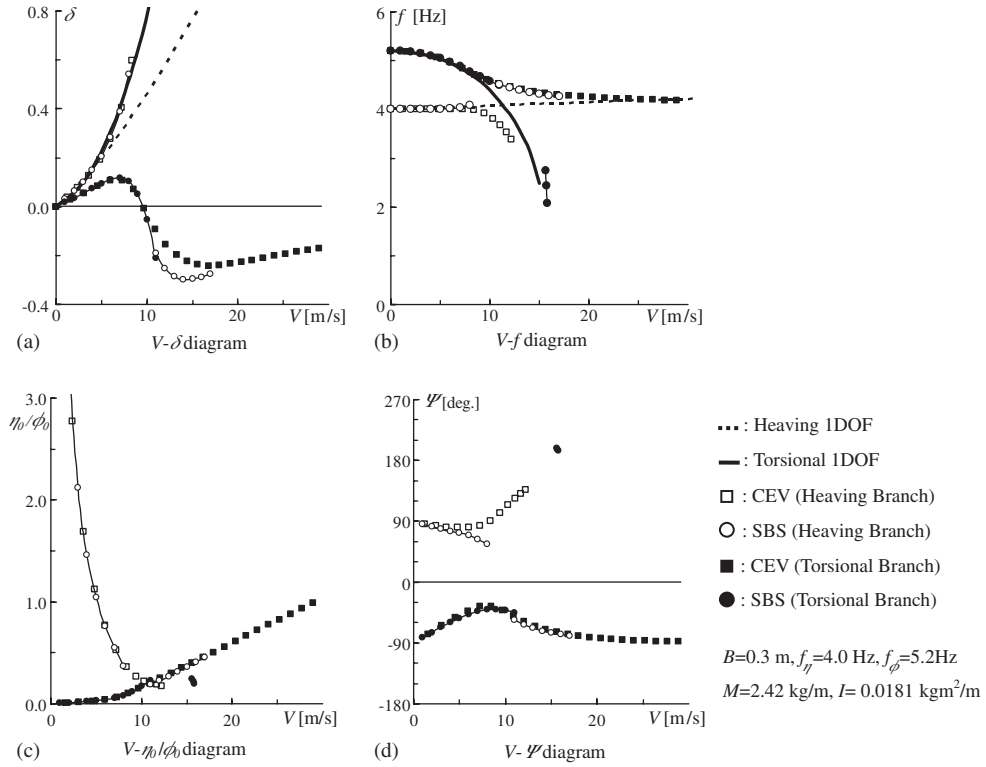

Fig. 6. Comparison of coupled flutter characteristics of thin plates, obtained by CEV and SBS analyses.

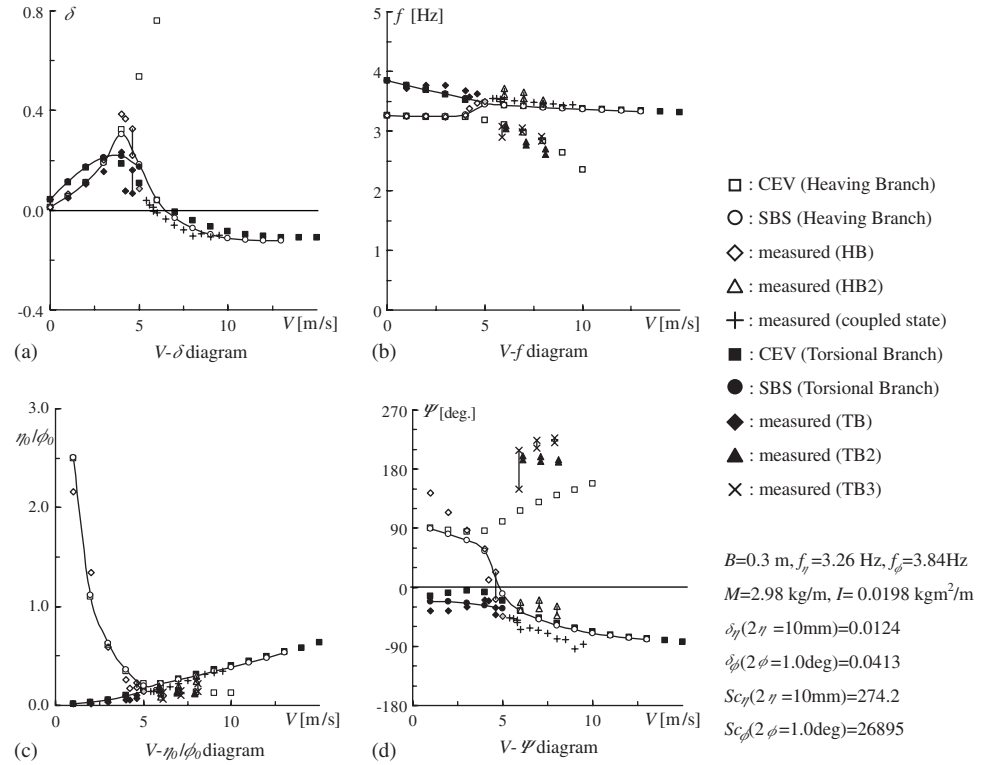

Fig. 7. Comparison of calculated coupled flutter characteristics for $B/D = 20$ rectangular cylinder, with those tested in free vibration test.

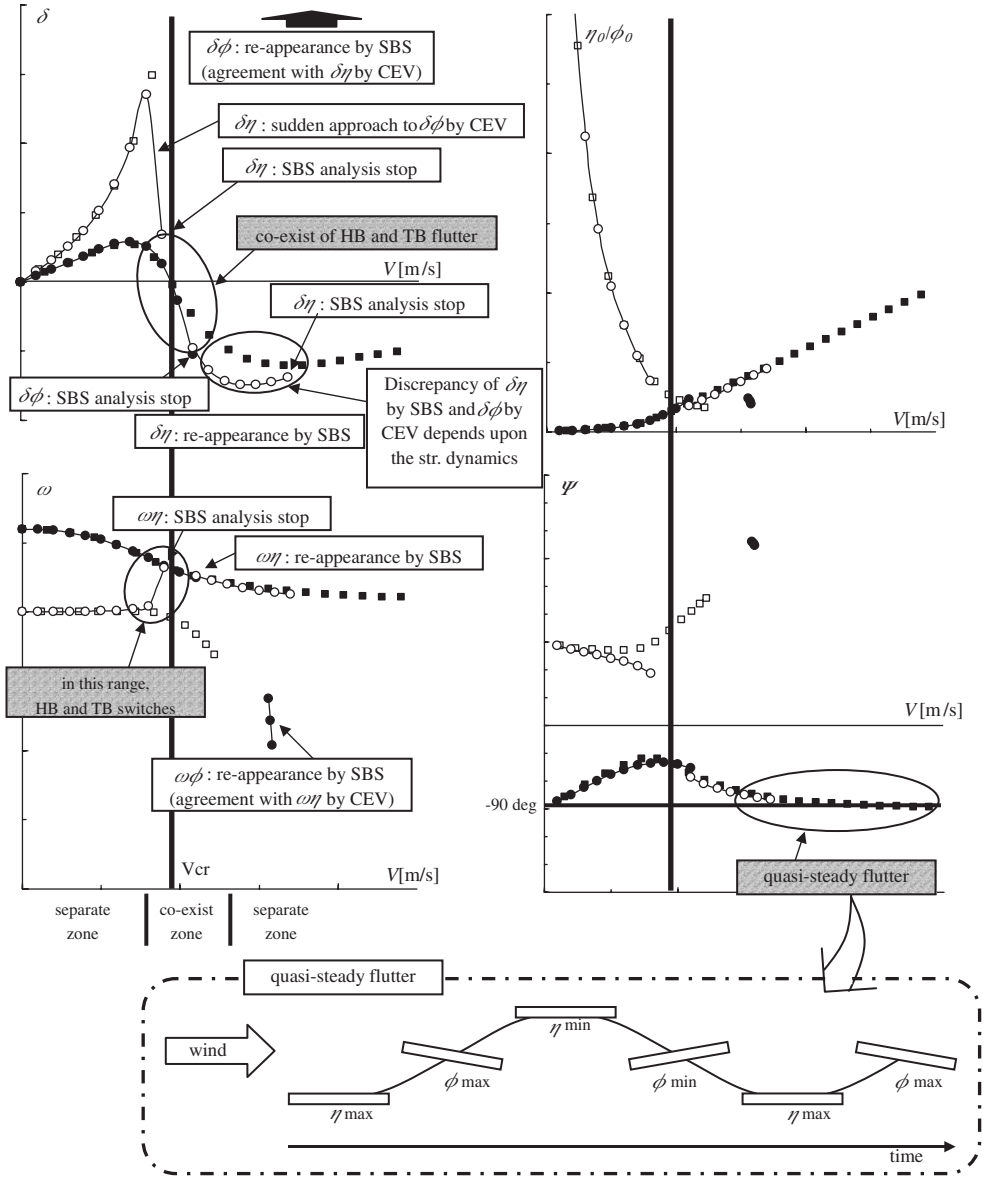

Fig. 8. Illustration of complicated branch switching in coupled flutter.

chord point. A_2^*, which has the characteristic of smoothly and continuously changing with B/D, while the flutter branch switch character is to abruptly change, if the torsional flutter is caused by TB.

3. Flutter branch characteristics of torsional flutter

Based on A_2^*characteristics for B/D ratios of 5, 8 and 10, rectangular cylinders show a torsional flutter instability in a torsional 1-dof system. However, the torsional flutter instability level decreases with B/D, as shown in Fig. 3. For cylinders that show torsional flutter instability, the coupled aerodynamic forces are generated by torsional and heaving motion, so that the coupled flutter instability may potentially exist, but is masked by torsional flutter instability. However, if the coupled flutter and the torsional flutter instability are compared from the aerodynamic instability point

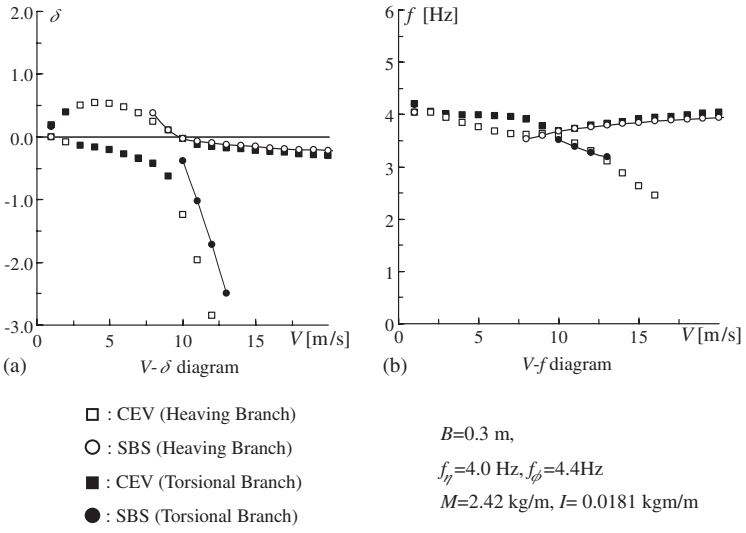

Fig. 9. Coupled flutter characteristics for $B/D = 5$ rectangular cylinder ($f_{\eta 0}/f_{\phi 0} = 1.1$), obtained by CEV analysis and SBS analysis.

of view, the torsional flutter, in general, must be unstable. On the other hand, if the torsional/heaving frequency ratio, $f_{\varphi 0}/f_{\eta 0}$, decreases, for example, from 1.7 to 1.1, then the coupled flutter becomes more unstable. In order to assess the possibility of a branch switch for a rectangular cylinder undergoing torsional flutter instability, CEV and SBS analyses were conducted for rectangular cylinders with B/D ratios of 5, 8 and 10, for frequency ratios, $f_{\varphi 0}/f_{\eta 0}$, of 1.1, 1.3 and 1.7. These analyses were performed for the same values of mass, mass inertia, cylinder dimension and torsional or heaving frequency. Torsional or heaving damping in still air was assumed as zero, since the fundamental flutter characteristics can be studied under these particular conditions. For a cylinder with B/D ratio of 5, torsional flutter occurs by TB for all frequency ratios (i.e., 1.1, 1.3 and 1.7), which is confirmed by the V–δ characteristics, but for the case of a frequency ratio of 1.1, it can be shown that the HB coupled flutter instability appears at high velocities, as shown in Fig. 9. The flutter characteristics obtained by CEV and SBS analysis almost coincide, despite the branch difference, even though the SBS result is not obtained at velocity ranges independent of the frequency ratio. On the other hand, for a cylinder with B/D ratio of 10 and a frequency ratio of 1.1, which is the case most sensitive to coupled flutter and the most insensitive to torsional flutter among the cylinders studied here, HB flutter appears through SBS analysis as if the flutter branch switches from TB to HB, which is obtained by CEV analysis at a velocity range of 5–15 m/s, as shown in Fig. 10. In this particular case, for the SBS analysis, the TB and HB frequency (f)–velocity (V) diagrams show the frequency crossing between TB and HB, similar to the coupled flutter case for a thin plate. By application of the case of the coupled flutter instability mechanism illustrated in Fig. 8, for this particular velocity range, TB flutter might co-exist with HB flutter. The flutter derivative contribution to HB flutter instability is mainly due to the absolute value of A_1^* and H_3^* as shown in Fig. 11. On the other hand, for a cylinder with a B/D ratio of 5, the HB damping characteristics are mostly characterized by H_1^* and the combination of A_4^* and the absolute value of H_3^*, corresponding to the flutter derivatives of the cylinder, which differ from those of the cylinders with B/D ratios of 8 and 10, described above.

4. Conclusion

The conclusions from this study on flutter branching in torsional flutter instability can be summarized as follows.

(i) Using SBS analysis, coupled flutter instability usually occurs by branch switching from the torsional branch (TB) to the heaving branch (HB), for higher velocity ranges.
(ii) The flutter branching characteristics of torsional flutter are, in general, more complicated than those for coupled flutter.
(iii) The flutter characteristics of the TB and the HB obtained by CEV and SBS analyses are fundamentally similar, but at particular wind velocity ranges they show certain discrepancies.

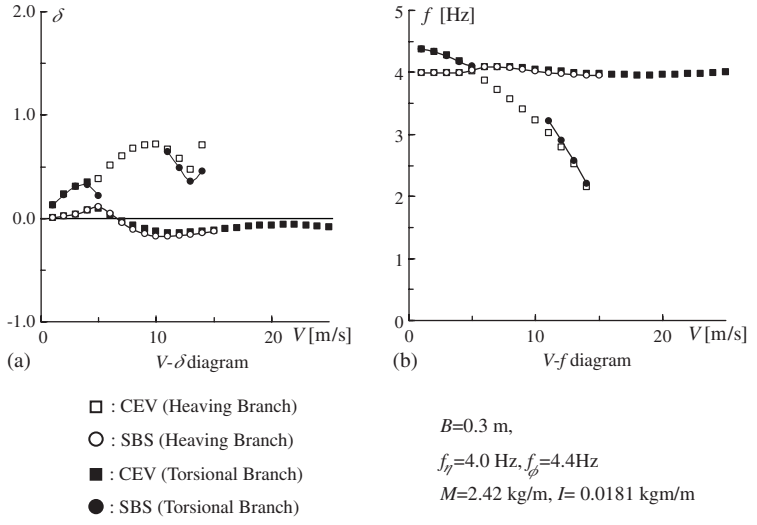

Fig. 10. Coupled flutter characteristics for $B/D = 10$ rectangular cylinder ($f_{\eta 0}/f_{\phi 0} = 1.1$), obtained by CEV analysis and SBS analysis.

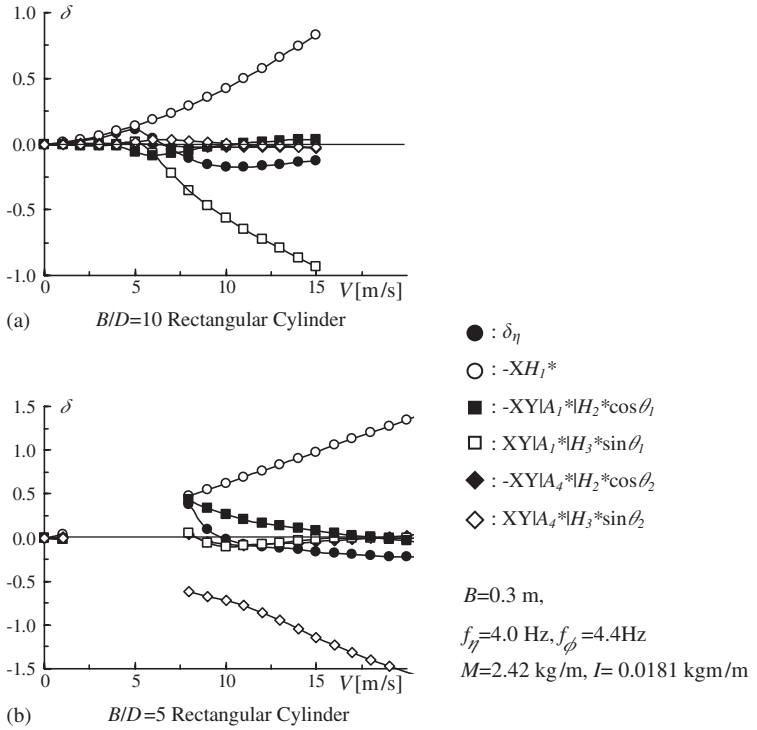

Fig. 11. Flutter derivative contribution to flutter instabilities, obtained by SBS analysis (HB); X and Y are defined in the text (Section 2.2).

(iv) The flutter branch characteristics of a cylinder with a B/D ratio of 5 are different from those of $B/D = 8$ and 10, because of differences in the flow field.

(v) In the case of torsional instability, the flutter branch is fundamentally torsional (TB), while the branch switch from the TB to the HB can be observed by SBS analysis in the case of a cylinder with a B/D ratio of 10, and a frequency ratio, $f_{\varphi 0}/f_{\eta 0}$, of 1.1, which is substantially similar to the coupled flutter branch switch.

(vi) Regarding the contribution of flutter derivatives to the TB and the HB, A_2^*, A_1^* and H_3^*, and H_1^*, A_1^* and H_3^* play major roles, respectively, for cylinders with B/D ratios of 8 and 10; while, on the other hand, for a cylinder with B/D ratio of 5 in the HB, H_1^*, A_4^* and H_3^* are the dominant variables.

(vii) SBS flutter analysis is a useful method for verifying the flutter branch characteristics for torsional flutter instability.

Lastly, it should be noted that experimental work is needed for comparison with the analytical results by SBS analysis—in particular for the case of a cylinder with a B/D ratio of 5 and a frequency ratio of 1.1, which would show the branch switch at lower velocity ranges.

References

von Karman, T., Sears, W.R., 1938. Airfoil theory for non-uniform motion. Journal of Aeronautical Sciences 5, 379–389.

Matsumoto, M., 1996. Aerodynamic damping of prisms. Journal of Wind Engineering and Industrial Aerodynamics 59, 159–175.

Matsumoto, M., Kobayashi, K., Niihara, Y., Shiarto, H., Hamasaki, H., 1995. Flutter mechanism and its stabilization of bluff bodies. In: Proceedings of the Ninth International Conference of Wind Engineering, pp. 827–838.

Matsumoto, M., Daito, Y., Yoshizumi, F., Ichikawa, Y., Yabutani, T., 1997a. Torsional flutter of bluff bodies. Journal of Wind Engineering and Industrial Aerodynamics 69–71, 871–882.

Matsumoto, M., Hamasaki, H., Yoshizumi, F., 1997b. On flutter stability of decks for super-long-span bridge. Japan Society of Civil Engineering, Structural Engineering/Earthquake Engineering 14, 185–199.

Scanlan, R.H., Tomko, J.J., 1971. Airfoil and bridge deck flutter derivatives. ASCE Journal of Engineering Mechanics Division 97, 1717–1737.

Theodorsen, T., 1935. General theory of aerodynamic instability and the mechanism of flutter. National Advisory Committee for Aeronautics, Technical Report 496, pp. 413–433.